Secondary Organic Aerosol Formation by Glyoxal Hydration and Oligomer Formation: Humidity Effects and Equilibrium Shifts During Analysis

*William P. Hastings, Charles A. Koehler, Earl L. Bailey, and David O. De Haan**

Chemistry Department, University of San Diego, 5998 Alcala Park, San Diego CA 92110

*corresponding author. (619) 260-6882. Fax: (619) 260-2211. e-mail: ddehaan@sandiego.edu

Supplementary Information

Contents:

13 pages including cover page

6 figures

2 mass spectrometer fragmentation schemes

SUPPLEMENTARY INFORMATION

GC injections of warm glyoxal trimer dihydrate (GTD) headspace. The behavior of glyoxal during GC analysis was studied by headspace injections from heated vials (~60°C) containing solid GTD. Helium (ultra pure, Air Gas Inc.) carrier gas (injection port pressure = 15 psi) and a HP-5 capillary column (30m × 0.25mm, 0.25 μm film thickness) were used in all runs. These injections consisted of volatilized glyoxal and water vapor. Resultant glyoxal peak heights and retention times depended strongly on injection port temperatures, rather than the GC oven initial temperature or temperature program. Results are summarized as a function of injection port temperatures in Figures A and B. When the GC injection port temperature was 120°C or less (with oven temperatures ramping from 80 to 120°C at 10 °C/min), extremely wide glyoxal peaks were observed that were incompletely eluted even after 15 minutes. When the GC injection port was set to more typical operating temperatures of 170°C or above (with initial oven temperatures ranging from 80 to 170°C in various runs), glyoxal was unretained and eluted with normal peak shapes. A clear trend of increasing signals at m/z = 58, the molecular glyoxal ion, is seen with respect to injection port temperature. In all cases, the injected headspace was generated by heating GTD at 60°C (a temperature too low to volatilize glyoxal hydrates or oligomers); thus, this data validates our method of producing glyoxal monomer. Since glyoxal monomer is injected with water vapor in the stoichiometric quantities necessary to form GTD, it appears that extensive yet reversible oligomer formation is possible at temperatures ≤ 120°C in GC injection ports. We reason that glyoxal oligomer formation does not occur in the column at oven temperatures as low as 80°C because of the slight chromatographic separation of glyoxal and water vapor.

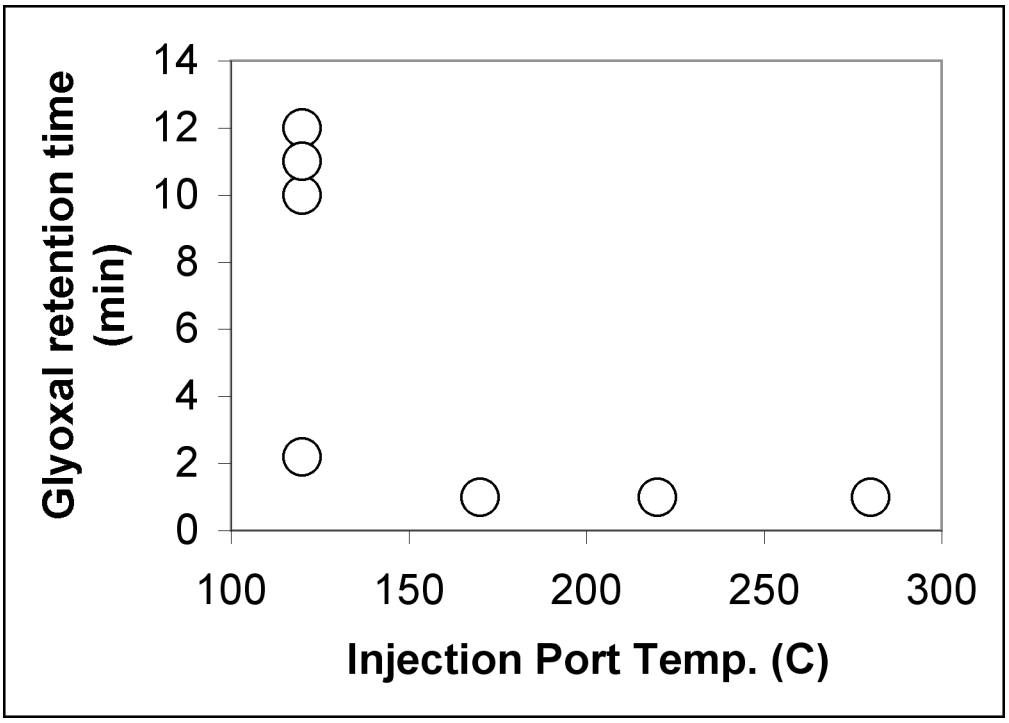

Figure A: Glyoxal retention times observed for gas-phase headspace injections from heated vials containing GTD, as a function of GC injection port temperature. Four runs were performed with the injection port at 220°C; in each case, glyoxal was unretained (t = 1 min). Other symbols represent single injections.

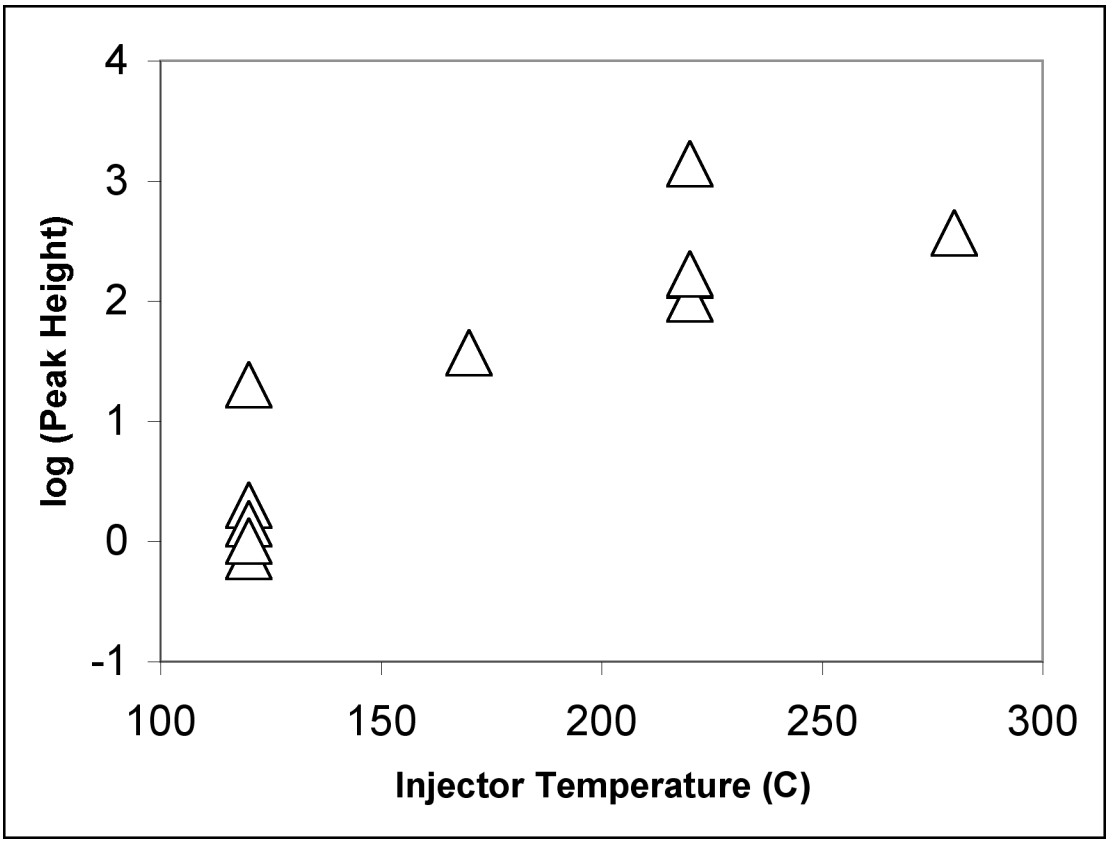

Figure B: Glyoxal peak heights (m/z = 58) for gas- phase headspace injections from heated vials containing GTD, as a function of GC injection port temperature.

Regardless of the injector temperature or the resulting elution time, the glyoxal mass spectra collected were nearly identical (e.g., Figure C). The ion chromatogram from a single ion monitoring run where the GC injection port temperature was increased from 120 to 230°C during the first 4 minutes of the run is shown in Figure D. Clearly, a form of glyoxal with low volatility had built up in the injection port from previous injections and was volatilized upon heating. In all ion chromatograms, including Figure D, ion peaks at 29, 30, 56 and 58 were perfectly correlated with each other and closely matched MS library *(1)* peak ratios for glyoxal (and also the glyoxal dimer). In our data, no ions at 28 (and little m/z = 18) were observed after baseline subtraction; these peaks in library spectra for glyoxal are not due to glyoxal or its oligomers. In

Figure D, it can be seen that as GC temperatures increase, ions 31 and 44 decayed more slowly than the other ions, and did not correlate with the other ions or even with each other. They are, however, present in the library spectra *(1)* for glyoxal and glyoxal dimer and are clearly associated with these compounds in our experiments. (The only difference between the NIST library spectra for glyoxal and the glyoxal dimer is a larger peak at m/z = 31 in the monomer spectrum. Neither spectra contains any ions heavier than the mass of glyoxal monomer.) The observed lack of correlation between the fragment ions present suggests that library mass spectra for glyoxal and glyoxal dimer contain peaks (m/z = 31 and 44) that are caused by interconversion during GC analysis. Furthermore, matches against these spectra (and indeed GC-MS mass spectra in general) cannot be used to differentiate between the forms of glyoxal originally injected into a hot GC injector.

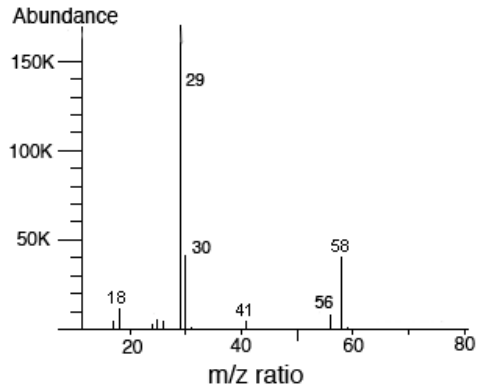

Figure C: Mass spectrum of glyoxal vapor at a retention time of 1.1 min, from a 2mL headspace injection from vial containing GTD at 60°C. Baseline subtraction has been performed to eliminate the spectral influence of nearby air peak. Abundances are scaled down by a factor of 10. GC injection port temperature: 280°C; oven temperature: 120°C; transfer line: 300°C.

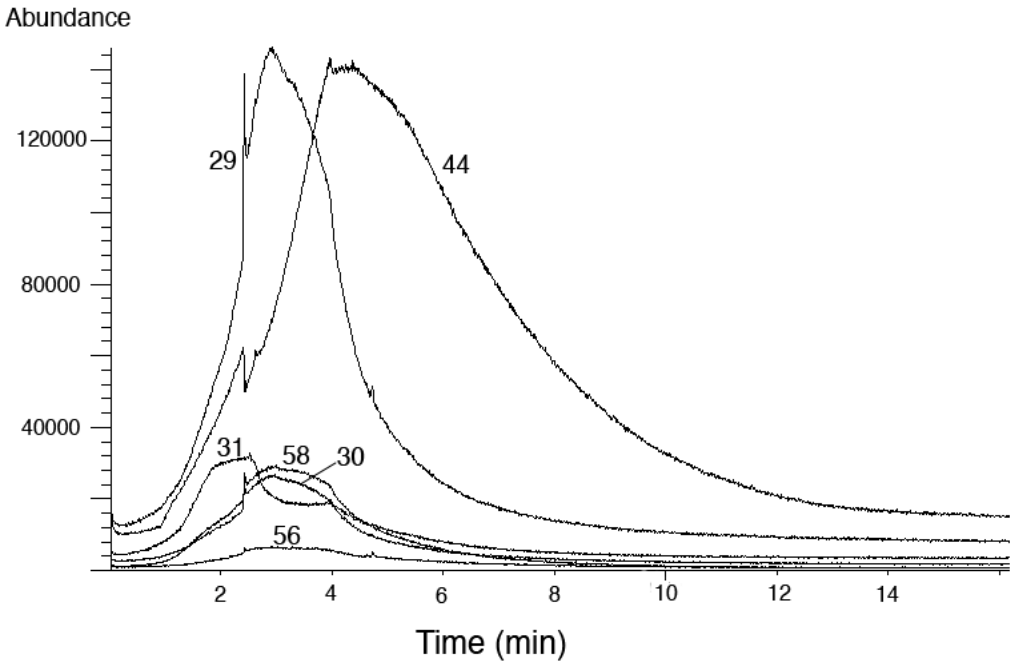

Figure D: Ion chromatogram taken as GC injection port, oven, and transfer line temperatures were ramped upward at maximum rate, starting at t = 0, after a series of GTD headspace and glyoxal hydrate injections in a cool (≤120°C) GC injection port. No further injection of glyoxal was performed at t = 0. Injection port temperature increased from 120 to 230°C in 4.2 min. Oven temperature increased from 80 to 230°C in 3 min. Transfer line temperature increased from 150 to 250 in 5.7 min.

The observed ions can be attributed to the fragments shown in Scheme 1. Ions 29, 30, and 56 can all be formed by simple fragmentation of glyoxal, m/z = 58, and so perfect correlation of these ions is reasonable. Ion 44, CO_2^+, can be formed either from oligomerized glyoxal, glyoxal monomer hydrate, or via substantial (and unlikely) rearrangement of the glyoxal monomer. Ion 31 can only be formed by substantial rearrangement of oligomerized glyoxal or glyoxal monomer hydrate, since a single glyoxal molecule lacks the three hydrogen atoms required to

form an ion of this mass. The prominent *m/z* = 31 peak in the NIST spectra of glyoxal *(1)*, but not the dimer, is therefore particularly unreasonable. Since the passage of an intact glyoxal dimer through the GC and into the ionization region of the MS seems unlikely because of its low vapor pressure, glyoxal monomer dihydrate (or monohydrate) is a more likely source for ion peaks at *m/z* = 31 and 44.

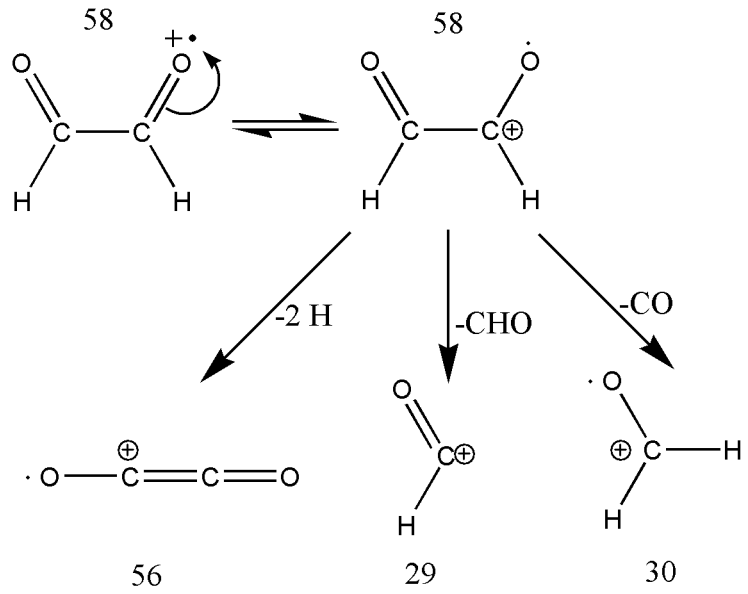

Other fragments:

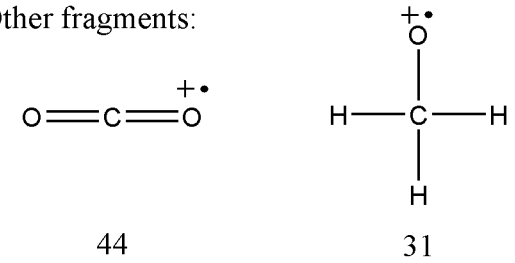

Scheme 1: Glyoxal monomer fragmentation

Electrospray ionization studies of glyoxal polymers. Although glyoxal oligomers will not pass through a GC without thermal breakdown, oligomers are easily observed by ESI-MS. Observed fragmentation pathways for glyoxal oligomers, performed by repeated fragmentation

in the ion trap mass spectrometer, are summarized in Figure E. As can be seen in Figure E, GTD (m/z = 210) fragments in the mass spectrometer via the sequential loss of four water molecules. Possible structures for these ions are shown in Scheme 2.

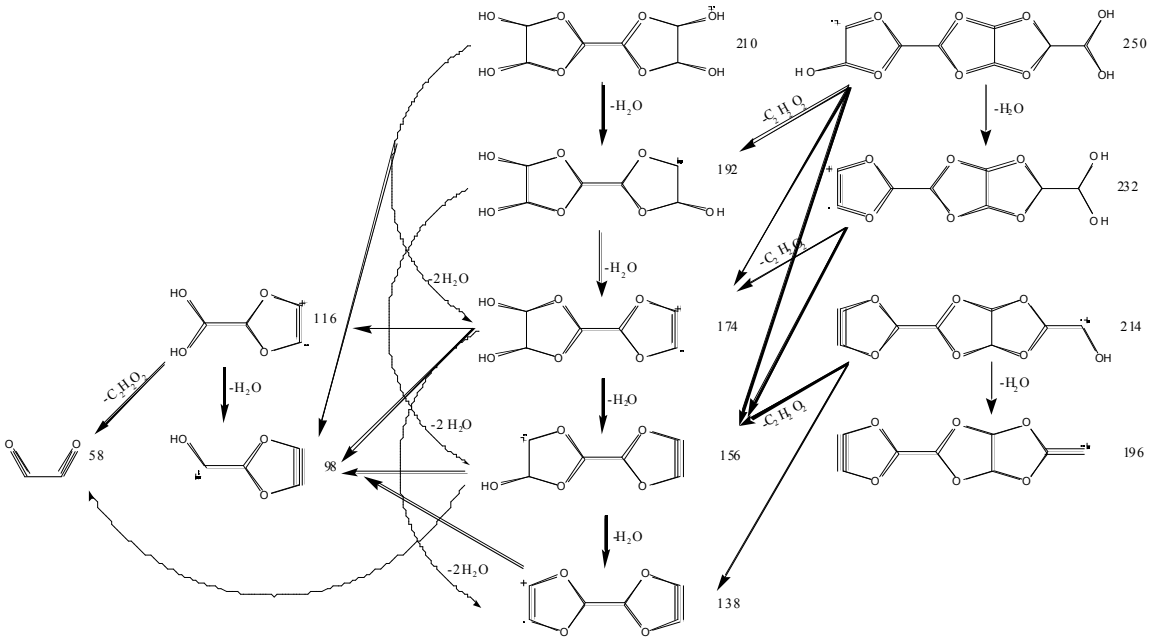

Figure E: Observed fragmentation pathways of glyoxal polymers caused by collisions in an ion trap mass spectrometer. Structures are best guesses of how multiple water moieties would be lost from glyoxal polymers connected entirely by five-membered dioxalane rings. Many other structural isomers are possible.

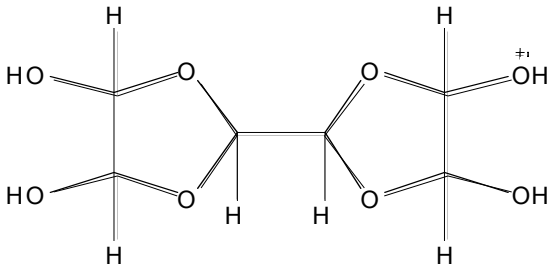

210

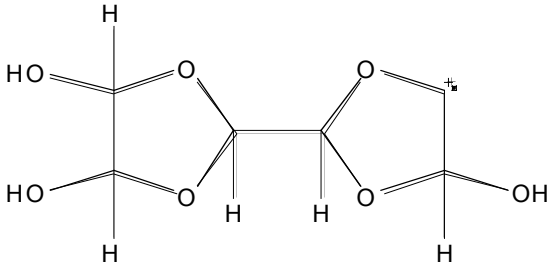

192

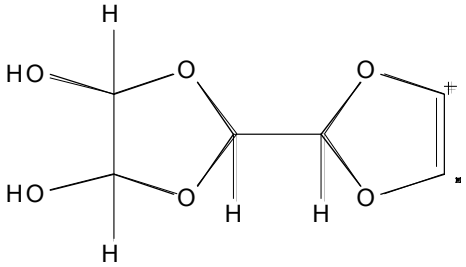

174

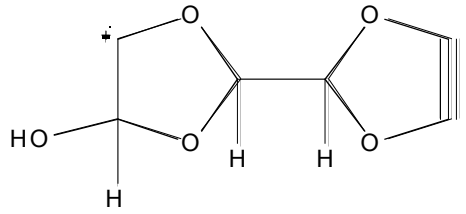

156

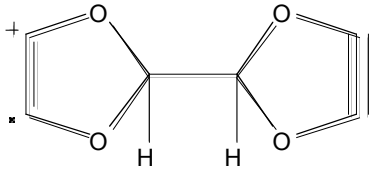

138

Scheme 2: Possible structures for observed MS fragments of GTD: sequential loss of four water moieties.

In order to quantify the effect of ESI-MS analysis on glyoxal polymerization equilibrium, the initial polymer equilibrium must be estimated. We assume that oligomer formation in a dilute aqueous phase is governed by the stepwise addition of glyoxal monomer hydrate:

$$\text{Glyoxal}_1 + \text{Glyoxal}_1 \leftrightarrow \text{Glyoxal}_2 + 2\ H_2O \qquad K_2 \qquad (3)$$

$$\text{Glyoxal}_1 + \text{Glyoxal}_n \leftrightarrow \text{Glyoxal}_{n+1} + 2\ H_2O \qquad K_{n+1} \qquad (4)$$

where *glyoxal*$_1$ is glyoxal monomer dihydrate, *glyoxal*$_2$ is glyoxal dimer dihydrate, and *glyoxal*$_n$ represents an oligomer dihydrate of *n* glyoxal units. We then assume that, as a first approximation, $K_{n+1} = K_2 = 0.56$, the value of K_2 at 25°C *(2)*. (It is likely that $K_{n+1} < K_2$, but we are trying to estimate the maximum expected concentrations of polymer.) The series of six equilibrium expressions (up to glyoxal$_7$) can be solved iteratively. Using this technique it is predicted that the equilibrium oligomer speciation in a 0.9 M aqueous glyoxal solution is 73% monomer dihydrate, 20% dimer dihydrate, and only 7% larger oligomers, as shown in Figure F. This distribution is in qualitative agreement with ^{13}C-NMR measurements *(3)*. It must be noted that this technique, while suitable for dilute aqueous phases, does not account for the decrease in solubility expected for large oligomers, and thus cannot be applied in non-dilute phases such as aerosol surface layers.

The 100-fold dilution of this solution in acetone (to 9 mM) before ESI-MS analysis would be expected to drop the rate of oligomer formation by a factor of ~10^4, since this rate is proportional to the concentration of the building blocks squared. The rate of oligomer hydrolysis should be proportional to the activity of water in solution, which declines by a factor of ~10^2 due to the dilution. Thus, while equilibrium is approached more slowly after the dilution, the expected equilibrium concentrations of glyoxal oligomers in the glyoxal / water / acetone solution

analyzed by ESI-MS is, if anything, even more skewed toward glyoxal monomer dihydrate than what is shown in Figure F.

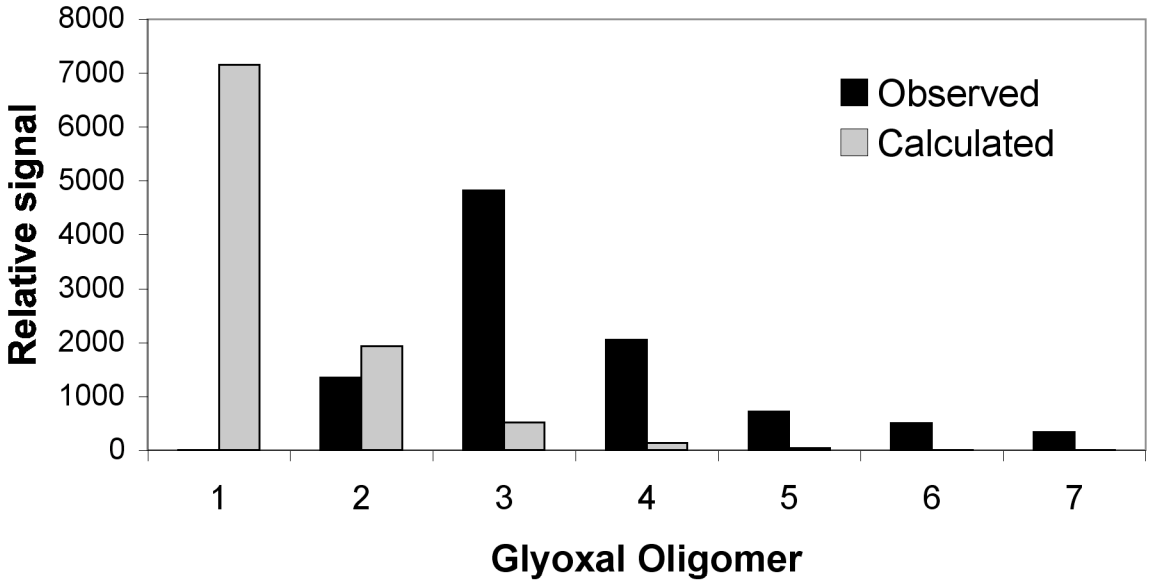

Figure F: Comparison of calculated (gray) and observed glyoxal oligomer distributions. Calculated distribution is for a 0.9 M aqueous glyoxal solution, assuming repeated addition of glyoxal monomer hydrate units, as described in the text. The total calculated oligomer distribution was scaled to match the total observed distribution. Observed distribution is based on attribution of mass spectral signals from Fig. 2, scaled down by a factor of 1000. Integrated peaks attributed to each oligomer are listed in Table 1. This data was recorded for the injection of a 100-fold acetone dilution of a 0.9 M aqueous glyoxal solution.

The peaks in Figure 2 were integrated to quantify observed oligomer speciation in the ESI-MS data. Integration areas of each peak assigned to a given oligomer (a row in Table 1) were

summed to find the total amount of signal attributable to each oligomer; these sums are also shown in Figure F. If we make the reasonably accurate assumptions that oligomers are ionized with similar efficiency, and that MS sensitivity is similar across the mass range, then peak areas are proportional to concentrations and our oligomer integration results can be directly compared to the calculated equilibrium oligomer distribution.

It is worth noting that any glyoxal oligomer that appears in the mass spectrum must have passed through the transfer capillary held at 150°C on the way into the MS without undergoing thermal breakdown. This is not surprising, however, since the oligomer is already charged and volatilized as it enters the capillary, and so passes through quickly. On the other hand, when a glyoxal oligomer is injected into a GC, it is deposited in a condensed phase on the hot injector liner, and has a contact time with this hot surface that is orders of magnitude longer, allowing extensive thermal breakdown to occur.

Particle chamber experiments. Humidified air was generated by bubbling air at 0.3 ml/min through a sintered glass inlet submerged in deionized water. The airflow then passed through a nylon membrane filter (pore size = 0.2 μm, Cole-Parmer) to remove any droplets formed in the bubbler. Relative humidity levels in the particle chamber were measured by a hygrometer (Fisher Scientific) located in the sampling port.

Accomodation coefficient calculations. The accommodation coefficient, α, is defined as the probability that a molecule colliding with a particle surface will be permanently incorporated into the particulate phase. Thus,

$$\alpha = \Phi_{net} / Z_w$$

where Φ_{net} is the net uptake rate per unit aerosol surface area (s^{-1}) and Z_w is the surface collision rate (s^{-1}). The uptake rate for a unit surface area is:

$$\Phi_{net} = G\ (1\ cm^2)\ \rho\ N_A / MW$$

where G = the particle diameter growth rate in cm/s, ρ is the density of glyoxal in the condensed phase, assumed to be equal to that of GTD (1.14 g/cm^3), N_A is Avogadro's number, and MW is the molar mass of glyoxal (58.04 g/mol). The surface collision rate, also for a unit surface area, is given by

$$Z_w = ¼\ C\ (8000RT/\pi MW)^{½}\ (1\ cm^2)$$

where C = gas phase concentration of glyoxal (molec/cm^3, constant throughout the gas phase since diffusion limitations were negligible), R is the gas constant (8.3145 J/mol K), and T is temperature (K).

References:

(1) NIST Standard Reference Database Number 69. National Institute of Standards and Technology, 2001, http://webbook.nist.gov/chemistry/

(2) Fratzke, A. R.; Reilly, P. J. Thermodynamic and kinetic analysis of the dimerization of aqueous glyoxal. *Intl. J. Chem. Kinet.* **1986**, *18* 775-789.

(3) Chastrette, F.; Bracoud, C.; Chastrette, M.; Mattioda, G.; Christidis, Y. Etude de la composition de solutions aqueuses de glyoxal en RMN-^{13}C. *Bull. Soc. Chim. Fr.* **1983** (1-2), II-33 - II-40.